Journal of Computational and Applied Mathematics 236 (2012) 3956–3966

Contents lists available at SciVerse ScienceDirect

Journal of Computational and Applied Mathematics

journal homepage: www.elsevier.com/locate/cam

A finite element frequency domain method for 2D photonic crystals

Pietro Contu, Cornelis van der Mee, Sebastiano Seatzu *

Dip. Matematica e Informatica, Università di Cagliari, Viale Merello 92, 09123 Cagliari, Italy

ARTICLE INFO

Article history:
Received 19 December 2011
Received in revised form 13 February 2012

In memory of Donato Trigiante

Keywords:
Photonic crystals
FEFD method
Circulant matrices

ABSTRACT

In this paper we propose a new finite element frequency domain (FEFD) method to compute the band spectra of 2D photonic crystals without impurities. Exploiting periodicity to identify discretization points differing by a period, it increases the effectiveness of the algorithm and reduces significantly its computational complexity. The results of an extensive experimentation indicate that our method offers an effective alternative to the most quoted methods in the literature.

1. Introduction

In this article we develop a finite element method for the Maxwell equations relevant to 2D photonic crystals [1,2] and employ the resulting generalized eigenvalue problems to determine their band spectra. In photonic crystals there is no accumulation of electric charge, no electric current and no magnetic material. As a consequence, assuming dielectric isotropy of the stationary medium and using harmonic modes, the Maxwell equations, which govern light transmission in photonic crystals, reduce to the following system of equations:

$$\nabla \cdot [\varepsilon \boldsymbol{E}] = 0, \quad \text{[Coulomb's law]} \tag{1.1a}$$

$$\nabla \times \boldsymbol{H} - i\kappa\varepsilon \boldsymbol{E} = 0, \quad \text{[Ampère's law]} \tag{1.1b}$$

$$\nabla \times \boldsymbol{E} + i\kappa \boldsymbol{H} = 0, \quad \text{[Faraday's law]} \tag{1.1c}$$

$$\nabla \cdot \boldsymbol{H} = 0. \quad \text{[Absence of free magnetic poles]} \tag{1.1d}$$

Here $\boldsymbol{E}$ and $\boldsymbol{H}$ are the electric and magnetic fields, ε is the dielectric constant (which depends on position $\boldsymbol{x} \in \mathbb{R}^2$ but not on time t), and the spectral parameter $\kappa = \frac{\omega}{c}$ is the ratio of the harmonic angular frequency ω and the lightspeed c. In 2D photonic crystals, the dielectric constant, for certain linearly independent vectors $\boldsymbol{a}_1, \boldsymbol{a}_2 \in \mathbb{R}^2$, satisfies the periodicity condition

$$\varepsilon(\boldsymbol{x} + m_1\boldsymbol{a}_1 + m_2\boldsymbol{a}_2) = \varepsilon(\boldsymbol{x}), \tag{1.2}$$

where m_1 and m_2 are arbitrary integers. In the 2D case the harmonic modes can be decomposed into two independent polarizations, the transverse magnetic (TM) mode and the transverse electric (TE) mode. In the TM mode the electric field ψ satisfies the Helmholtz equation [3]

$$-\nabla^2\psi = \eta\varepsilon\psi, \tag{1.3}$$

* Corresponding author. Tel.: +39 0706755619; fax: +39 0706755601.
E-mail addresses: contu22@interfree.it (P. Contu), cornelis@krein.unica.it (C. van der Mee), seatzu@unica.it (S. Seatzu).

0377-0427/$ – see front matter © 2012 Elsevier B.V. All rights reserved.
doi:10.1016/j.cam.2012.02.041

whereas in the TE mode the magnetic field ψ satisfies

$$-\nabla\cdot\left(\frac{1}{\varepsilon}\nabla\psi\right)=\eta\psi. \tag{1.4}$$

In (1.3) and (1.4), $\eta=\kappa^2$ is the spectral parameter allowing one to identify the band spectra and the field ψ points in the z-direction and only depends on $(x,y)\in\mathbb{R}^2$. Using the Bloch representation

$$\psi(\boldsymbol{x},\boldsymbol{k})=e^{i\boldsymbol{k}\cdot\boldsymbol{x}}\phi(\boldsymbol{x},\boldsymbol{k}),$$

where the wavevector $\boldsymbol{k}$ belongs to the first Brillouin zone [4] and ϕ satisfies the periodicity condition

$$\phi(\boldsymbol{x}+m_1\boldsymbol{a}_1+m_2\boldsymbol{a}_2,\boldsymbol{k})=\phi(\boldsymbol{x},\boldsymbol{k}) \tag{1.5}$$

for any $m_1, m_2\in\mathbb{Z}$, we obtain instead of (1.3) and (1.4) the equation

$$-\nabla^2\phi-2i\boldsymbol{k}\cdot\nabla\phi+\|\boldsymbol{k}\|^2\phi=\eta\varepsilon\phi \tag{1.6}$$

for TM modes and the equation

$$-\nabla\cdot\left(\frac{1}{\varepsilon}\nabla\phi\right)-i\nabla\cdot\left(\frac{1}{\varepsilon}\boldsymbol{k}\phi\right)-i\frac{1}{\varepsilon}\boldsymbol{k}\cdot\nabla\phi+\frac{\|\boldsymbol{k}\|^2}{\varepsilon}\phi=\eta\phi \tag{1.7}$$

for TE modes. In (1.6) and (1.7), as throughout the paper, $\|\cdot\|$ denotes the Euclidean norm. Our goal is to find the eigenvalues η as a function of $\boldsymbol{k}$ varying in the first Brillouin zone.

Several numerical methods have been proposed for the solution of the Maxwell equations in the case of 1D, 2D and 3D periodic dielectric media. Depending on the problem, algorithms working either in the time or frequency domain or algorithms working in real or reciprocal space have been proposed. Among the frequency domain methods, we refer to the Fourier expansion (FE) method [1,5,6], the finite difference frequency domain (FDFD) method [7,8], and the finite element frequency domain (FEFD) method [9–17]. From what we know, all of the FEFD methods proposed so far have a higher computational complexity than the FE and FEFD methods proposed in [1,7], respectively. The reason is probably due to an inefficient use of the periodicity conditions. The method presented here is the only FEFD method that exploits these conditions efficiently, converting the initial problem into a generalized eigenvalue problem whose matrices are strongly structured. As a consequence, it allows us to increase the accuracy of the computation of spectral bands, as well as to reduce its computational complexity. More precisely, choosing positive integers n, m and the division points

$$\boldsymbol{x}_{j,l}=(j/n)\boldsymbol{a}_1+(l/m)\boldsymbol{a}_2,\quad (j,l)\in\mathbb{Z}^2, \tag{1.8}$$

as in [7], we can convert the FEFD method for the TM and TE cases into linear systems of the type

$$(A-\eta B)\boldsymbol{\phi}=0, \tag{1.9}$$

where A and B are sparse positive definite matrices of order nm. As a consequence, our method approximates η by solving the generalized eigenvalue problem (1.9).

The outline of the paper is as follows: in Section 2, we illustrate the implementation of our method in the rectangular and oblique 2D crystal cases. Section 3 is devoted to the analysis of the generalized eigenvalue problem to solve, while in Section 4 we present the results of extensive numerical experimentation. These results have been obtained by using our FEFD method and by comparing them with those obtained by using both our FDFD method [7] and the FE method of Joannopoulos et al. [1], which is the most quoted and used method in the photonic crystals area. Section 5 is devoted to our conclusions.

2. Finite element frequency domain (FEFD)

In this section we illustrate the finite element method that we developed in the frequency domain to compute the spectra of 2D photonic crystals. As far as the notation is concerned we refer to [18].

a. Rectangular case. Setting $\boldsymbol{A}=\{t_1\boldsymbol{a}_1+t_2\boldsymbol{a}_2:0\le t_1,t_2<1\}$, let us define the complex Hilbert spaces H_{per} and H^1_{per} consisting of those measurable complex-valued functions ϕ on $\mathbb{R}^2$ which satisfy the periodicity condition (1.5) and are finite with respect to the following respective squared norms:

$$\|\phi\|^2_{H_{\text{per}}}=\iint_{\boldsymbol{A}}dxdy\,|\phi(x,y)|^2,$$

$$\|\phi\|^2_{H^1_{\text{per}}}=\iint_{\boldsymbol{A}}dxdy(|\phi(x,y)|^2+\|\nabla\phi(x,y)\|^2).$$

As a consequence of the first Green identity and the periodicity condition, we see that $\phi\in H^1_{\text{per}}$ is a variational solution to (1.6) (TM mode) if

$$\iint_{\boldsymbol{A}}dxdy\{\nabla\phi\cdot\nabla v^*-2i[\boldsymbol{k}\cdot\nabla\phi]v^*+\|\boldsymbol{k}\|^2\phi v^*-\eta\varepsilon\phi v^*\}=0, \tag{2.1}$$

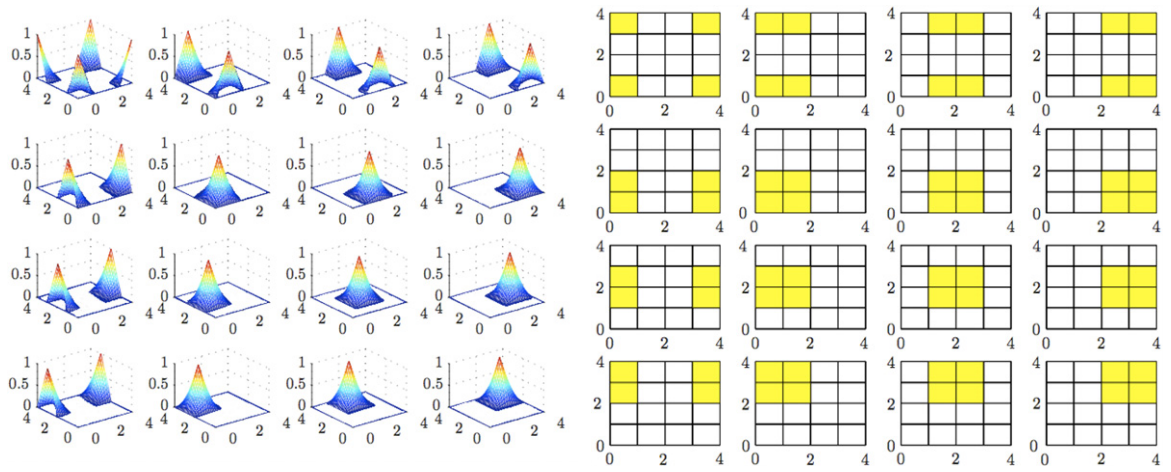

Fig. 1. In the left half of the figure some periodic linear spline functions (2.3) are displayed and in the right half their support in the case of a 4×4 regular mesh.

for every $v \in H^1_{\mathrm{per}}$. Analogously, we call $\phi \in H^1_{\mathrm{per}}$ a distributional solution to (1.7) (TE mode) if

$$\iint_{\boldsymbol{A}} dxdy \left\{ \frac{1}{\varepsilon} \nabla\phi \cdot \nabla v^* - iv^* \boldsymbol{k} \cdot \nabla \left(\frac{1}{\varepsilon} \phi \right) - \frac{i}{\varepsilon} v^* \boldsymbol{k} \cdot \nabla\phi + \frac{\|\boldsymbol{k}\|^2}{\varepsilon} \phi v^* - \eta \phi v^* \right\} = 0, \tag{2.2}$$

for every $v \in H^1_{\mathrm{per}}$.

Restricting ourselves to rectangular 2D crystals where $\boldsymbol{a}_1 = (a, 0)$ and $\boldsymbol{a}_2 = (0, b)$, and putting $h_x = (a/n)$, $h_y = (b/m)$, we interpolate $\phi \in H^1_{\mathrm{per}}$ as follows:

$$\Phi_{j,l}(x, y) = \sum_{s=-\infty}^{\infty} \sum_{\sigma=-\infty}^{\infty} \varphi \left(\frac{x - x_{ns+j,m\sigma+l}}{h_x} \right) \varphi \left(\frac{y - y_{ns+j,m\sigma+l}}{h_y} \right), \tag{2.3}$$

where $\boldsymbol{x}_{ns+j,m\sigma+l} = (x_{ns+j,m\sigma+l}, y_{ns+j,m\sigma+l})$ and

$$\varphi(x) = \begin{cases} 1 - |x|, & -1 \le x \le 1, \\ 0, & x \le -1 \text{ or } x \ge 1, \end{cases}$$

is a linear spline supported on $[-1, 1]$ (Fig. 1). Then each function $\Phi_{j,l}(x, y)$ belongs to H^1_{per} and satisfies the periodicity conditions

$$\Phi_{j+n,l}(x, y) = \Phi_{j,l+m}(x, y) = \Phi_{j,l}(x, y), \quad (j, l) \in \mathbb{Z}^2.$$

Furthermore, $\{\Phi_{j,l}(x, y) : (j, l) \in \mathbb{Z}^2\}$ is a partition of unity in the sense that

$$\sum_{j=-\infty}^{\infty} \sum_{l=-\infty}^{\infty} \Phi_{j,l}(x, y) = 1, \quad (x, y) \in \mathbb{R}^2.$$

Let us denote by $\mathcal{S}_{n,m}$ the nm-dimensional subspace of H^1_{per} spanned by the linear spline functions $\Phi_{j,l}(x, y)$ ($j = 0, 1, \ldots, n-1$, $l = 0, 1, \ldots, m-1$), and let us write down the variational equations (2.1) and (2.2) for $\phi, v \in \mathcal{S}_{n,m}$. Substituting

$$\phi(x, y) = \sum_{j'=0}^{n-1} \sum_{l'=0}^{m-1} \phi_{j',l'} \Phi_{j',l'}(x, y)$$

and $v = v^* = \Phi_{j,l}$, from (2.1) we obtain the linear system (TM mode) of order nm

$$\sum_{j'=0}^{n-1} \sum_{l'=0}^{m-1} \phi_{j',l'} \int_0^a dx \int_0^b dy \, \{(\nabla\Phi_{j',l'} + i\Phi_{j',l'}\boldsymbol{k}) \cdot (\nabla\Phi_{j,l} - i\Phi_{j,l}\boldsymbol{k})\}$$

$$= \eta \sum_{j'=0}^{n-1} \sum_{l'=0}^{m-1} \phi_{j',l'} \int_0^a dx \int_0^b dy \, \varepsilon(x, y) \Phi_{j',l'}(x, y) \Phi_{j,l}(x, y) \tag{2.4}$$

whose unknowns are the values of $\phi(x, y)$ at the interpolation points of the photonic cell $0 \le x \le a$, $0 \le x \le b$. From (2.2) (TE mode) we obtain instead

$$\sum_{j'=0}^{n-1}\sum_{l'=0}^{m-1}\phi_{j',l'}\int_0^a\int_0^b \frac{dx\,dy}{\varepsilon(x,y)}\{(\nabla\Phi_{j',l'}+i\Phi_{j',l'}\boldsymbol{k})\cdot(\nabla\Phi_{j,l}-i\Phi_{j,l}\boldsymbol{k})\}$$

$$=\eta\sum_{j'=0}^{n-1}\sum_{l'=0}^{m-1}\phi_{j',l'}\int_0^a dx\int_0^b dy\,\Phi_{j',l'}(x,y)\Phi_{j,l}(x,y). \tag{2.5}$$

The linear systems (2.4) and (2.5) constitute the finite element schemes to compute the eigenvalues η for fixed wavevector $\boldsymbol{k}$ for the TM and TE modes, respectively.

In the homogeneous case ($\varepsilon(x, y) \equiv \varepsilon$ constant) the generalized linear systems (2.4) and (2.5) coincide when we consider a regular grid ($h_x = h_y = h$) on a square domain ($a = b$). In this case the corresponding matrices A and B of (1.9) have the following structured forms:

$$A=\left(\begin{array}{cccc|cccc|cccc|cccc}
\alpha & \beta_2 & 0 & \beta_2^* & \beta_1 & \gamma_1 & 0 & \gamma_2 & 0 & 0 & 0 & 0 & \beta_1^* & \gamma_2^* & 0 & \gamma_1^* \\
\beta_2^* & \alpha & \beta_2 & 0 & \gamma_2 & \beta_1 & \gamma_1 & 0 & 0 & 0 & 0 & 0 & \gamma_1^* & \beta_1^* & \gamma_2^* & 0 \\
0 & \beta_2^* & \alpha & \beta_2 & 0 & \gamma_2 & \beta_1 & \gamma_1 & 0 & 0 & 0 & 0 & 0 & \gamma_1^* & \beta_1^* & \gamma_2^* \\
\beta_2 & 0 & \beta_2^* & \alpha & \gamma_1 & 0 & \gamma_2 & \beta_1 & 0 & 0 & 0 & 0 & \gamma_2^* & 0 & \gamma_1^* & \beta_1^* \\
\hline
\beta_1^* & \gamma_2^* & 0 & \gamma_1^* & \alpha & \beta_2 & 0 & \beta_2^* & \beta_1 & \gamma_1 & 0 & \gamma_2 & 0 & 0 & 0 & 0 \\
\gamma_1^* & \beta_1^* & \gamma_2^* & 0 & \beta_2^* & \alpha & \beta_2 & 0 & \gamma_2 & \beta_1 & \gamma_1 & 0 & 0 & 0 & 0 & 0 \\
0 & \gamma_1^* & \beta_1^* & \gamma_2^* & 0 & \beta_2^* & \alpha & \beta_2 & 0 & \gamma_2 & \beta_1 & \gamma_1 & 0 & 0 & 0 & 0 \\
\gamma_2^* & 0 & \gamma_1^* & \beta_1^* & \beta_2 & 0 & \beta_2^* & \alpha & \gamma_1 & 0 & \gamma_2 & \beta_1 & 0 & 0 & 0 & 0 \\
\hline
0 & 0 & 0 & 0 & \beta_1^* & \gamma_2^* & 0 & \gamma_1^* & \alpha & \beta_2 & 0 & \beta_2^* & \beta_1 & \gamma_1 & 0 & \gamma_2 \\
0 & 0 & 0 & 0 & \gamma_1^* & \beta_1^* & \gamma_2^* & 0 & \beta_2^* & \alpha & \beta_2 & 0 & \gamma_2 & \beta_1 & \gamma_1 & 0 \\
0 & 0 & 0 & 0 & 0 & \gamma_1^* & \beta_1^* & \gamma_2^* & 0 & \beta_2^* & \alpha & \beta_2 & 0 & \gamma_2 & \beta_1 & \gamma_1 \\
0 & 0 & 0 & 0 & \gamma_2^* & 0 & \gamma_1^* & \beta_1^* & \beta_2 & 0 & \beta_2^* & \alpha & \gamma_1 & 0 & \gamma_2 & \beta_1 \\
\hline
\beta_1 & \gamma_1 & 0 & \gamma_2 & 0 & 0 & 0 & 0 & \beta_1^* & \gamma_2^* & 0 & \gamma_1^* & \alpha & \beta_2 & 0 & \beta_2^* \\
\gamma_2 & \beta_1 & \gamma_1 & 0 & 0 & 0 & 0 & 0 & \gamma_1^* & \beta_1^* & \gamma_2^* & 0 & \beta_2^* & \alpha & \beta_2 & 0 \\
0 & \gamma_2 & \beta_1 & \gamma_1 & 0 & 0 & 0 & 0 & 0 & \gamma_1^* & \beta_1^* & \gamma_2^* & 0 & \beta_2^* & \alpha & \beta_2 \\
\gamma_1 & 0 & \gamma_2 & \beta_1 & 0 & 0 & 0 & 0 & \gamma_2^* & 0 & \gamma_1^* & \beta_1^* & \beta_2 & 0 & \beta_2^* & \alpha
\end{array}\right), \tag{2.6}$$

where, setting $k^2 = k_x^2 + k_y^2$,

$$\alpha = \frac{8}{3}+\frac{4}{9}k^2h^2,$$

$$\beta_1 = -\frac{1}{3}+\frac{1}{9}k^2h^2-\frac{2}{3}ik_yh, \qquad \beta_1^* = -\frac{1}{3}+\frac{1}{9}k^2h^2+\frac{2}{3}ik_yh,$$

$$\beta_2 = -\frac{1}{3}+\frac{1}{9}k^2h^2-\frac{2}{3}ik_xh, \qquad \beta_2^* = -\frac{1}{3}+\frac{1}{9}k^2h^2+\frac{2}{3}ik_xh,$$

$$\gamma_1 = -\frac{1}{3}+\frac{1}{36}k^2h^2-i\frac{(k_x+k_y)h}{6}, \qquad \gamma_1^* = -\frac{1}{3}+\frac{1}{36}k^2h^2+i\frac{(k_x+k_y)h}{6},$$

$$\gamma_2 = -\frac{1}{3}+\frac{1}{36}k^2h^2+i\frac{(k_x-k_y)h}{6}, \qquad \gamma_2^* = -\frac{1}{3}+\frac{1}{36}k^2h^2-i\frac{(k_x-k_y)h}{6},$$

and

$$B=\left(\begin{array}{cccc|cccc|cccc|cccc}
a & b & 0 & b & b & c & 0 & c & 0 & 0 & 0 & 0 & b & c & 0 & c \\
b & a & b & 0 & c & b & c & 0 & 0 & 0 & 0 & 0 & c & b & c & 0 \\
0 & b & a & b & 0 & c & b & c & 0 & 0 & 0 & 0 & 0 & c & b & c \\
b & 0 & b & a & c & 0 & c & b & 0 & 0 & 0 & 0 & c & 0 & c & b \\
\hline
b & c & 0 & c & a & b & 0 & b & b & c & 0 & c & 0 & 0 & 0 & 0 \\
c & b & c & 0 & b & a & b & 0 & c & b & c & 0 & 0 & 0 & 0 & 0 \\
0 & c & b & c & 0 & b & a & b & 0 & c & b & c & 0 & 0 & 0 & 0 \\
c & 0 & c & b & b & 0 & b & a & c & 0 & c & b & 0 & 0 & 0 & 0 \\
\hline
0 & 0 & 0 & 0 & b & c & 0 & c & a & b & 0 & b & b & c & 0 & c \\
0 & 0 & 0 & 0 & c & b & c & 0 & b & a & b & 0 & c & b & c & 0 \\
0 & 0 & 0 & 0 & 0 & c & b & c & 0 & b & a & b & 0 & c & b & c \\
0 & 0 & 0 & 0 & c & 0 & c & b & b & 0 & b & a & c & 0 & c & b \\
\hline
b & c & 0 & c & 0 & 0 & 0 & 0 & b & c & 0 & c & a & b & 0 & b \\
c & b & c & 0 & 0 & 0 & 0 & 0 & c & b & c & 0 & b & a & b & 0 \\
0 & c & b & c & 0 & 0 & 0 & 0 & 0 & c & b & c & 0 & b & a & b \\
c & 0 & c & b & 0 & 0 & 0 & 0 & c & 0 & c & b & b & 0 & b & a
\end{array}\right), \tag{2.7}$$

where

$$a = \frac{4}{9}h^2, \qquad b = \frac{1}{9}h^2, \qquad c = \frac{1}{36}h^2.$$

Both matrices A and B are Hermitian sparse and block-circulant whose blocks are circulant matrices as well. The same conclusions hold true if $a \neq b$ and the mesh decomposition is not uniform ($h_x \neq h_y$). In the inhomogeneous case, A is as before for the TM modes while B is not block-circulant and conversely, for the TE modes, B is block-circulant as in (2.7) and A is not block-circulant.

b. Oblique case. If the 2D photonic crystal is oblique, we make the coordinate transformation

$$\boldsymbol{x} = \mathrm{col}(\boldsymbol{a}^1, \boldsymbol{a}^2)\boldsymbol{\xi} = \begin{pmatrix} a_{11} & a_{21} \\ a_{12} & a_{22} \end{pmatrix} \begin{pmatrix} \xi \\ \zeta \end{pmatrix} = A^T\boldsymbol{\xi}, \tag{2.8}$$

where ξ and ζ are orthogonal coordinates and $\boldsymbol{a}^1$ and $\boldsymbol{a}^2$ denote the transposed rows of A. The finite element schemes for the TM and TE modes are easily found by applying the coordinate transformation (2.8) to (2.4) and (2.5), where the integration is performed over the parallelogram $\boldsymbol{A}$ instead of $[0, a] \times [0, b]$. Omitting the obvious definitions of $\tilde{\phi}_{j,l}$ and $\tilde{\Phi}_{j,l}$, we get instead of (2.4) (TM mode)

$$\begin{aligned} &\sum_{j'=0}^{n-1}\sum_{l'=0}^{m-1} \tilde{\phi}_{j',l'} \int_0^1 d\xi \int_0^1 d\zeta \left\{ \left(\frac{\boldsymbol{b}_1 \cdot \nabla_{\boldsymbol{\xi}} \tilde{\Phi}_{j',l'}}{2\pi}\boldsymbol{i} + \frac{\boldsymbol{b}_2 \cdot \nabla_{\boldsymbol{\xi}} \tilde{\Phi}_{j',l'}}{2\pi}\boldsymbol{j} + i\tilde{\Phi}_{j',l'}\boldsymbol{k} \right) \right. \\ &\quad \left. \times \left(\frac{\boldsymbol{b}_1 \cdot \nabla_{\boldsymbol{\xi}} \tilde{\Phi}_{j,l}}{2\pi}\boldsymbol{i} + \frac{\boldsymbol{b}_2 \cdot \nabla_{\boldsymbol{\xi}} \tilde{\Phi}_{j,l}}{2\pi}\boldsymbol{j} - i\tilde{\Phi}_{j,l}\boldsymbol{k} \right) \right\} \\ &= \eta \sum_{j'=0}^{n-1}\sum_{l'=0}^{m-1} \tilde{\phi}_{j',l'} \int_0^1 d\xi \int_0^1 d\zeta\, \tilde{\varepsilon}(\xi, \zeta)\tilde{\Phi}_{j',l'}(\xi, \zeta)\tilde{\Phi}_{j,l}(\xi, \zeta), \end{aligned} \tag{2.9}$$

where $\boldsymbol{i} = (1, 0)^T$ and $\boldsymbol{j} = (0, 1)^T$.

Moreover, instead of (2.5) (TE mode) we get

$$\begin{aligned} &\sum_{j'=0}^{n-1}\sum_{l'=0}^{m-1} \tilde{\phi}_{j',l'} \int_0^1 \int_0^1 \frac{d\xi\, d\zeta}{\tilde{\varepsilon}(\xi, \zeta)} \left\{ \left(\frac{\boldsymbol{b}_1 \cdot \nabla_{\boldsymbol{\xi}} \tilde{\Phi}_{j',l'}}{2\pi}\boldsymbol{i} + \frac{\boldsymbol{b}_2 \cdot \nabla_{\boldsymbol{\xi}} \tilde{\Phi}_{j',l'}}{2\pi}\boldsymbol{j} + i\tilde{\Phi}_{j',l'}\boldsymbol{k} \right) \right. \\ &\quad \left. \times \left(\frac{\boldsymbol{b}_1 \cdot \nabla_{\boldsymbol{\xi}} \tilde{\Phi}_{j,l}}{2\pi}\boldsymbol{i} + \frac{\boldsymbol{b}_2 \cdot \nabla_{\boldsymbol{\xi}} \tilde{\Phi}_{j,l}}{2\pi}\boldsymbol{j} - i\tilde{\Phi}_{j,l}\boldsymbol{k} \right) \right\} \\ &= \eta \sum_{j'=0}^{n-1}\sum_{l'=0}^{m-1} \tilde{\phi}_{j',l'} \int_0^1 d\xi \int_0^1 d\zeta\, \tilde{\Phi}_{j',l'}(\xi, \zeta)\tilde{\Phi}_{j,l}(\xi, \zeta). \end{aligned} \tag{2.10}$$

In this case, as in the rectangular case, the initial problem has been converted in the generalized eigenvalue problem (1.9). As far as the structure of the matrices A and B is concerned, the conclusions are as in the rectangular case.

3. Analysis of the matrix systems

The linear systems (2.4) (TM rectangular), (2.5) (TE rectangular), (2.9) (TM oblique), and (2.10) (TE oblique), obtained by applying our method, have the form

$$(A - \eta B)\boldsymbol{\phi} = 0, \tag{3.1}$$

where A is a nonnegative Hermitian matrix and B is a positive definite Hermitian matrix, both of order mn.

The linear system (3.1) is derived by applying the variational principles (2.1) (TM mode) and (2.2) (TE mode) to ϕ, v belonging to a suitable mn-dimensional subspace of H^1_{per}.

Since the minimax characterization of the eigenvalues is also valid for (2.1) and (2.2), we easily see that the first eigenvalue of (2.4), (2.5), (2.9) and (2.10) is larger than (or coincides with) the first eigenvalue of the corresponding variational problem (2.1) or (2.2). In particular, these numerical principles imply that the matrices A and B in (3.1) are nonnegative Hermitian and strictly positive Hermitian, respectively. Unless $k_x = k_y = 0$, in which case $\eta = 0$ is an eigenvalue, the matrix A has only positive eigenvalues.

Let us now consider the detailed structure of the matrices A and B obtained by applying our FEFD method. The supports of the spline functions $\Phi_{j,l}(x, y)$ and $\Phi_{j',l'}(x, y)$ have an intersection of positive measure if and only if $j - j' \in \{0, 1, -1, n - 1, 1 - n\}$ and $l - l' \in \{0, 1, -1, m - 1, 1 - m\}$. To make this statement more evident, we displayed in Fig. 1 some translates of the periodic linear spline (2.3) and the corresponding supports.

This implies that the two-index matrices A and B appearing in the linear systems (2.4)–(2.10), obtained by applying the FEFD method, are two-index tridiagonal matrices in the sense that their elements $A_{(j,l),(j',l')}$ and $B_{(j,l),(j',l')}$ vanish whenever either $j - j' \notin \{0, 1, -1, n-1, 1-n\}$ or $l - l' \notin \{0, 1, -1, m-1, 1-m\}$.

The matrices A in (2.4) and (2.9) (TM mode) and the matrices B in (2.5) and (2.10) (TE mode) are also two-index circulant matrices, in the sense that $A_{(j,l),(j',l')}$ and $B_{(j,l),(j',l')}$ only depend on the remainders of $j - j'$ and $l - l'$ upon division by n and m, respectively. In all four cases considered, the matrix A is nonnegative Hermitian and the matrix B is positive definite Hermitian.

In homogeneous media ($\varepsilon(x, y) \equiv \varepsilon$ constant) the eigenvalues can be explicitly obtained by resorting to the symbols associated to the circulant matrices A and B, both in the rectangular and in the oblique case. In fact [19–21], it can be proved that their generalized eigenvalues are given by

$$\hat{c}(z, w; \boldsymbol{k}) = \frac{\hat{a}(z, w; \boldsymbol{k})}{\hat{b}(z, w; \boldsymbol{k})}, \tag{3.2}$$

where $\hat{a}(z, w; \boldsymbol{k})$ and $\hat{b}(z, w; \boldsymbol{k})$ are the symbols of A and B, respectively, associated to $\boldsymbol{k}$ and $z^n = 1$ and $z^m = 1$.

Let us consider, for the sake of simplicity, the square case ($a = b$) and uniform mesh ($h_x = h_y = h$). In this case

$$\hat{a}(z, w; \boldsymbol{k}) = (\alpha + \beta_2 z + \bar{\beta}_2 z^{-1}) + (\beta_1 + \gamma_1 z + \gamma_2 z^{-1})w + (\bar{\beta}_1 + \bar{\gamma}_2 z + \bar{\gamma}_1 z^{-1})w^{-1}$$

and

$$\hat{b}(z, w; \boldsymbol{k}) = (a + bz + bz^{-1}) + (b + cz + cz^{-1})w + (b + cz + cz^{-1})w^{-1}.$$

Writing $z = e^{i\theta_j}$ with $\theta_j = \frac{2\pi j}{n}$ and $w = e^{i\varphi_l}$ with $\varphi_l = \frac{2\pi l}{m}$, we can write the symbols in the form

$$\begin{aligned}\hat{a}(e^{i\theta_j}, e^{i\varphi_l}; \boldsymbol{k}) \;=\; & \frac{2}{3}(4 - \cos\theta_j - \cos\varphi_l - 2\cos\theta_j\cos\varphi_l) + \frac{h^2}{9}(2 + \cos\theta_j) \\ & \times (2 + \sin\varphi_l)k^2 + \frac{2}{3}hk_x \sin\theta_j(2 + \cos\varphi_l) + \frac{2}{3}hk_y \sin\varphi_l(2 + \cos\theta_j),\end{aligned} \tag{3.3}$$

$$\hat{b}(e^{i\theta_j}, e^{i\varphi_l}; \boldsymbol{k}) = \frac{h^2}{9}(2 + \cos\theta_j)(2 + \sin\varphi_l), \tag{3.4}$$

where $j, l = 0, 1, \ldots, n-1$, n being the number of mesh points along the x and y axes.

It can be shown that

$$\frac{\hat{a}(e^{i\theta_j}, e^{i\varphi_l}; \boldsymbol{k})}{\hat{b}(e^{i\theta_j}, e^{i\varphi_l}; \boldsymbol{k})} = \left(k_x + \frac{2\pi j}{a}\right)^2 + \left(k_y + \frac{2\pi l}{a}\right)^2 + O\left(\frac{1}{n^2}\right). \tag{3.5}$$

If $a \neq b$ and $h_x \neq h_y$, the right hand side of (3.5) becomes $(k_x + \frac{2\pi j}{a})^2 + (k_y + \frac{2\pi l}{b})^2 + O(\frac{1}{n^2} + \frac{1}{m^2})$, where n and m are the number of mesh points along the x and y axes, respectively. As a result of the nonnegativity of the matrices A and B, the symbols $\hat{a}(e^{i\theta_j}, e^{i\varphi_l}; \boldsymbol{k})$ and $\hat{b}(e^{i\theta_j}, e^{i\varphi_l}; \boldsymbol{k})$ are nonnegative, irrespective of the choice of h_x, h_y, k_x and k_y.

The symbol computation in the oblique homogeneous case is a straightforward generalization of that in the rectangular case and gives results similar to (3.5), i.e. the numerical eigenvalues tend to the exact eigenvalues apart from an $O(n^{-2}+m^{-2})$ term.

4. Numerical results

In this section we present the most significant numerical results of an extensive experimentation involving the band spectra of 2D photonic crystals, carried out by using our FEFD method. These results are compared with those obtained by using both our FDFD method proposed in [7] and the MIT Photonic-Bands software [22].

All computations in this paper were performed using MatLab (version 7.11.0) on an AMD46 computer equipped with an Intel Core i7 860 processor with a speed of 2.80 GHz.

4.1. 2D band spectra

The photonic crystal configurations considered in this section are those depicted in Fig. 2 in the case of a rectangular lattice, in Fig. 3 in the case of an oblique lattice, both considered before in [1], and in Fig. 4. More precisely, denoting by a the lattice constant, we considered the following configurations of photonic crystals:

(a) a square distribution of dielectric rods ($\varepsilon = 8.9$, radius $r = 0.2a$) embedded in air (top half of Fig. 2);
(b) a square distribution of dielectric veins ($\varepsilon = 8.9$, thickness $0.165a$) embedded in air (bottom half of Fig. 2);
(c) a triangular array of air columns drilled in a dielectric substrate (radius $r = 0.48a$, $\varepsilon = 13$), (Fig. 3);
(d) a square distribution of concentric dielectric rods ($\varepsilon_{1,2,3} = 2, 3, 4$, radii $r_{1,2,3} = 0.4a, 0.3a, 0.2a$) embedded in air (Fig. 4).

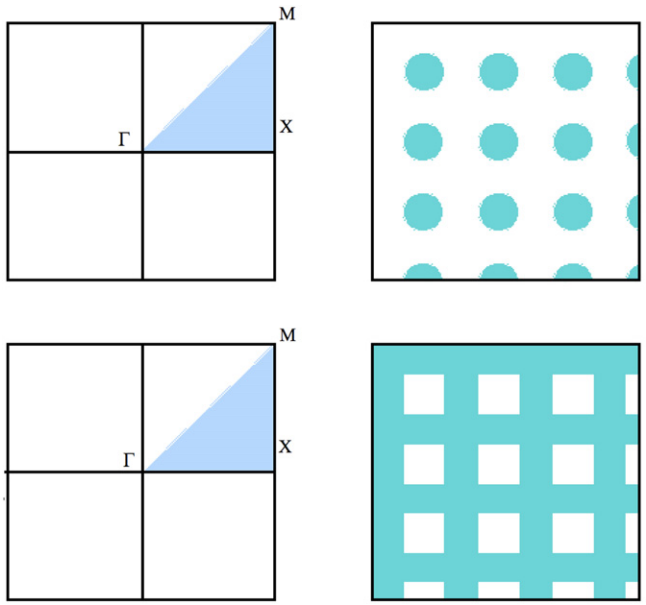

Fig. 2. The top half of the figure shows a photonic crystal composed of a square distribution of dielectric rods ($\varepsilon = 8.9, r = 0.2a$) embedded in air and the corresponding Brillouin zone. The Γ-point corresponds to $k_x = k_y = 0$, the X-point to $k_x = \pi/a$ and $k_y = 0$ and the M-point to $k_x = k_y = \pi/a$, a being either period. The bottom half of the figure shows a photonic crystal composed of a square distribution of dielectric veins ($\varepsilon = 8.9$, thickness $0.165a$) in air and the corresponding Brillouin zone.

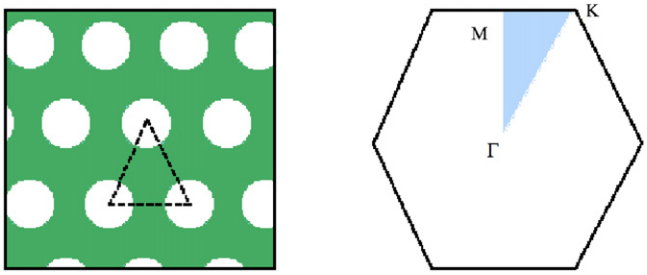

Fig. 3. The figure shows a photonic crystal made of a triangular array of air columns drilled in a dielectric substrate ($r = 0.48a$, $\varepsilon = 13$) and the corresponding Brillouin zone. The Γ-point corresponds to $k_x = k_y = 0$, the M-point to $k_x = 0$ and $k_y = 2\pi/(\sqrt{(3)}a)$ and the K-point to $k_x = 2\pi/(3a)$ and $k_y = 2\pi/(\sqrt{(3)}a)$, where the period parallelogram is a rhombus with sides a.

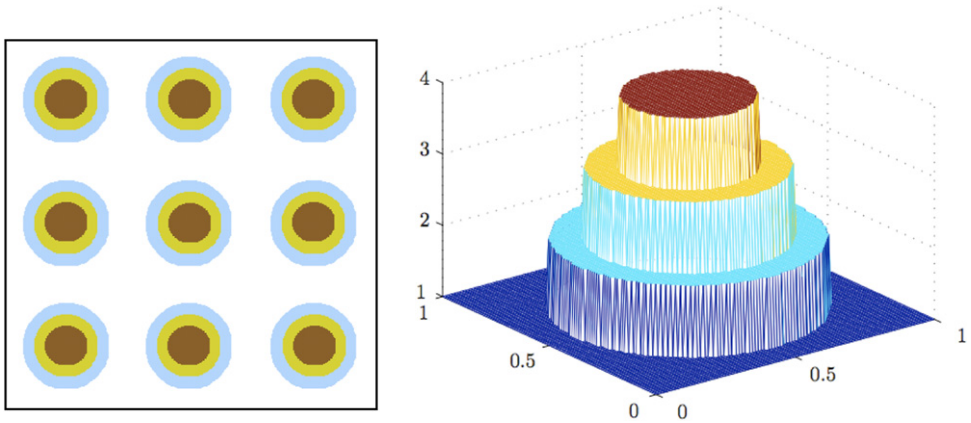

Fig. 4. The figure on the left shows a photonic crystal made of a square distribution of concentric dielectric rods ($\varepsilon_{1,2,3} = 2, 3, 4$, radii $r_{1,2,3} = 0.4a, 0.3a, 0.2a$) embedded in air, while the figure on the right shows a 3D representation of its fundamental cell where the heights of the dielectric constants $\varepsilon_{1,2,3}$ are reported on the z-axis.

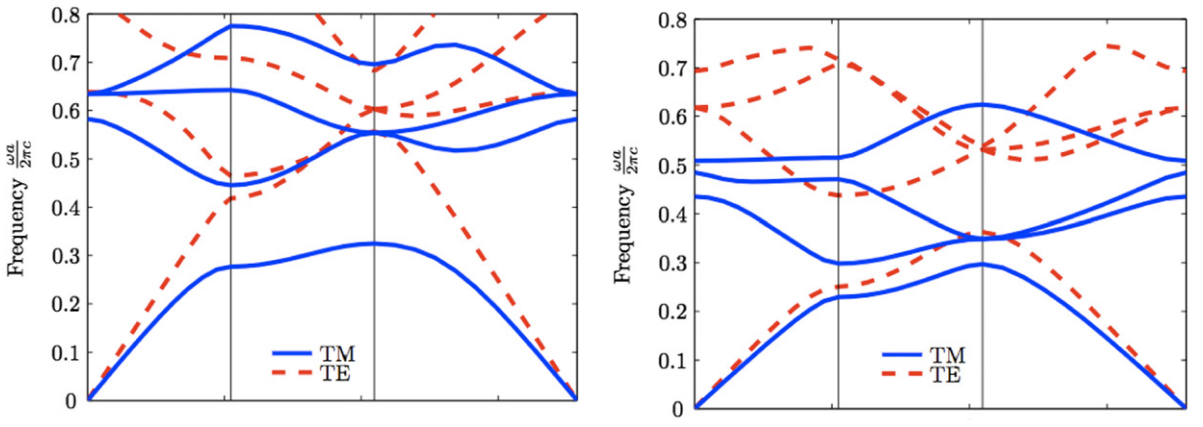

Fig. 5. The figure on the left shows the lowest TM and TE spectra obtained by our FEFD method for a square array of dielectric columns in air (top half of Fig. 2) and on the right for a square array of dielectric veins in air (bottom half of Fig. 2).

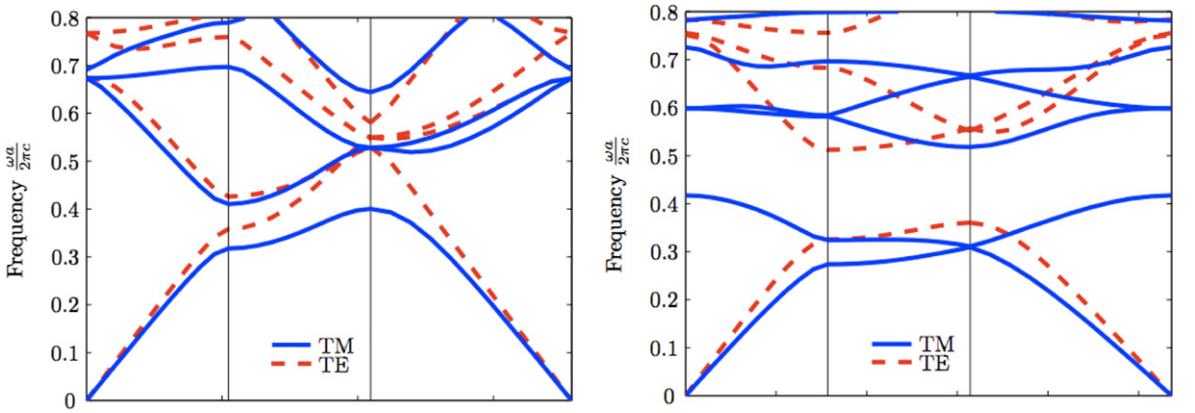

Fig. 6. The Figure on the left shows the lowest TM and TE spectra obtained by our FEFD method for a square array of dielectric concentric columns in air (Fig. 4), while the figure on the right shows the lowest TM and TE spectra for a photonic crystal made of a triangular distribution of rods embedded in a dielectric medium (Fig. 3).

The photonic cell described in (d) has been introduced to extend the comparison among the results obtained by our FDFD and FEFD methods and the FE method by using the mentioned MIT Photonic-Bands software [1].

In the rectangular case the band spectrum has been computed by solving the generalized eigenvalue problems (2.4), (2.5). Since $\varepsilon(\boldsymbol{x})$ is invariant under the group of automorphisms of the square lattice, it is sufficient to consider one eighth of the Brillouin zone [4] (Fig. 2). Therefore we solve the eigenvalue problems varying $\boldsymbol{k}$ on the boundary of the colored region shown in Figs. 2 and 3. More precisely, we consider the following (k_x, k_y) values:

1. $k_x \in [0, \pi/a],\ k_y = 0,$
2. $k_x = \pi/a,\ k_y \in [0, \pi/a],$
3. $k_x \in [0, \pi/a],\ k_y \in [0, \pi/a],$

in the rectangular case (Fig. 2) and the following (k_x, k_y) values:

1. $k_x = 0,\ k_y \in [0, 2\pi/(\sqrt{3}a)],$
2. $k_x \in [0, 2\pi/(3a)],\ k_y = 2\pi/(\sqrt{3}a),$
3. $k_x \in [2\pi/(3a), 0],\ k_y \in [2\pi/(\sqrt{3}a), 0],$

in the oblique case (Fig. 3). The 2D band spectra thus obtained are shown in Figs. 5 and 6. The numerical results are in good agreement with both the FDFD method [7] and the FE method [1].

In order to assess the effectiveness of our method, let us now preliminarily consider the homogeneous media case ($\varepsilon(x, y) \equiv \varepsilon$ constant) where, for a fixed wavevector $\boldsymbol{k}$, the exact expression of the (j, l)-th eigenvalue is as follows:

$$\eta_{(j,l;\boldsymbol{k})} = \left(\frac{2\pi j}{a} + k_x\right)^2 + \left(\frac{2\pi l}{b} + k_y\right)^2.$$

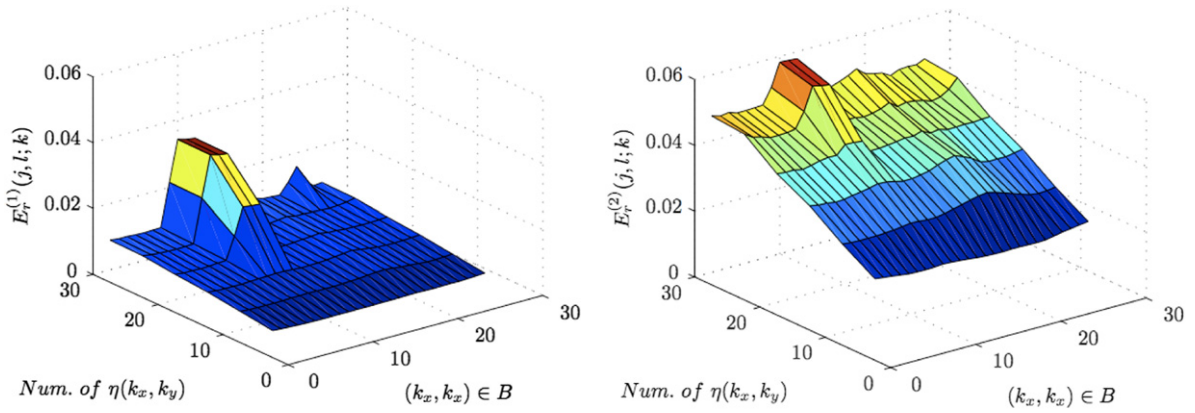

Fig. 7. The figures show the relative errors $E_r^{(1)}(j,l;\boldsymbol{k})$ (left) and $E_r^{(2)}(j,l;\boldsymbol{k})$ (right) for a photonic crystal made of a cylindrical distribution of dielectric ($\varepsilon = 8.9$) in air for TM modes.

Denoting by $\eta(j,l;\boldsymbol{k})$ the exact (j,l)-th eigenvalue corresponding to the fixed wavevector $\boldsymbol{k}$ and by $\hat{\eta}(j,l;\boldsymbol{k})$ its numerical estimate, we consider the relative error $E_r(j,l;\boldsymbol{k})$ and the relative Euclidean norm of the stack ordered errors $E_e(j,l;\boldsymbol{k})$ as follows

$$E_r(j,l;\boldsymbol{k}) = \frac{|\hat{\eta}_{(j,l;\boldsymbol{k})} - \eta_{(j,l;\boldsymbol{k})}|}{|\eta_{(j,l;\boldsymbol{k})}|}, \qquad E_e(j,l;\boldsymbol{k}) = \frac{\|\mathrm{vec}(\hat{\eta}_{(j,l;\boldsymbol{k})} - \eta_{(j,l;\boldsymbol{k})})\|}{\|\mathrm{vec}(\eta_{(j,l;\boldsymbol{k})})\|},$$

and compute their maximal values for each fixed $\boldsymbol{k}$ vector, for $j = 0, 1, \ldots, n-1$ and $l = 0, 1, \ldots, m-1$. The numerical results, obtained by considering a regular grid of 256×256 points, have been compared with those obtained by considering the same grid points in the FDFD method and in the above MIT Photonic-Band software.

The reference to such grid parameters is due to our numerical experiments, which highlight that with these settings the execution times for the estimates of the 30 smallest eigenvalues are essentially the same. In fact, fixing a tolerance value τ for such relative errors, our numerical tests show that the minimal time necessary to have a relative error lower than τ, for each fixed wavevector $\boldsymbol{k}$, is essentially the same. Setting $E_r = \max[E_r(j,l;\boldsymbol{k})]$ and $E_e = \max[E_e(j,l;\boldsymbol{k})]$, where $\boldsymbol{k}$ varies in the first Brillouin zone and (j,l) as before specified, we obtained:

	FEFD	FDFD	FE-MIT
$10^4 E_r$	3.2281	2.3764	2.0461
$10^4 E_e$	1.7570	1.4325	0.4197
CPU time (s)	423.03	308.52	393.18

In the inhomogeneous case we computed the 30 smallest eigenvalues using our FEFD and FDFD methods and calculated their distance from the corresponding smallest eigenvalues obtained by using the MIT Photonic-Band software mentioned above. More precisely, for each $\boldsymbol{k}$ chosen in the first Brillouin zone, we computed the following relative errors

$$E_r^{(1)}(j,l;\boldsymbol{k}) = \frac{\|\eta^{FDFD}_{(j,l;\boldsymbol{k})} - \eta^{FE-MIT}_{(j,l;\boldsymbol{k})}\|}{\|\eta^{FE-MIT}_{(j,l;\boldsymbol{k})}\|}, \qquad E_r^{(2)}(j,l;\boldsymbol{k}) = \frac{\|\eta^{FEFD}_{(j,l;\boldsymbol{k})} - \eta^{FE-MIT}_{(j,l;\boldsymbol{k})}\|}{\|\eta^{FE-MIT}_{(j,l;\boldsymbol{k})}\|}$$

for 5 successive eigenvalues (1–5, 6–10, …, 25–30). We then plot $E_r^{(1)}(j,l;\boldsymbol{k})$ and $E_r^{(2)}(j,l;\boldsymbol{k})$ as the values of a surface having the chosen $\boldsymbol{k}$ as the x-axis and the multiples of the 5 smallest eigenvalues on the y-axis. All cases considered in this paper show, for roughly the same computing time, that $E_r^{(1)}(j,l;\boldsymbol{k}) \leq E_r^{(2)}(j,l;\boldsymbol{k})$ with differences among them that are irrelevant from the applicational point of view. As an example, we displayed in Fig. 7 and in Fig. 8 such surfaces for the TM and TE modes, respectively, when the photonic crystal consists of a cylindrical distribution of dielectric medium in air. These figures, as well as the analogous figures that we have considered in our experimentation, show that the effectiveness of each of the three methods that we analyzed is essentially the same.

5. Conclusions

Our numerical experiments give numerical evidence of substantial effectiveness among the three methods considered at almost the same computational complexity. In fact, our numerical computations show that the 10 smallest eigenvalues, obtained by the three methods, are essentially the same, as shown in Table 1 for a particular structure and a particular wavevector. The emphasis on these eigenvalues is due to their relevance in the physical application, as the literature [1] makes it evident.

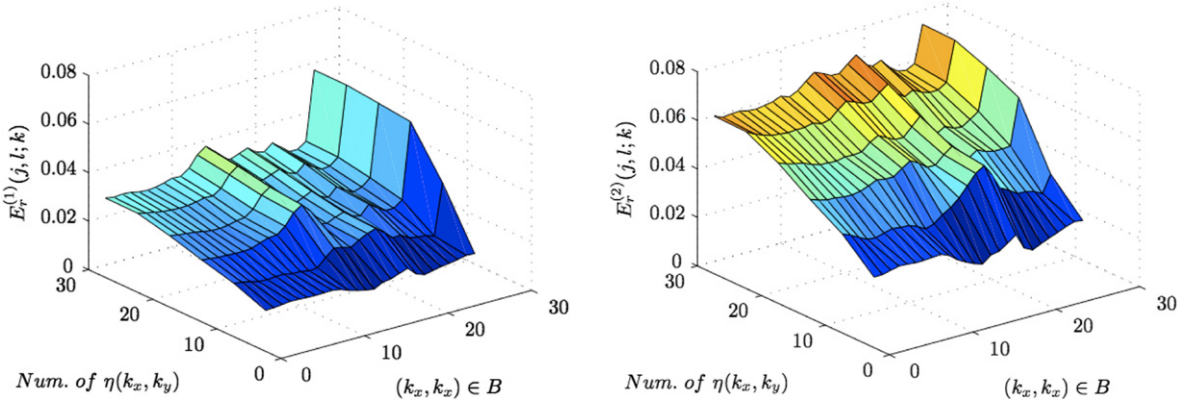

Fig. 8. The figures show the relative errors of $E_r^{(1)}(j, l; \boldsymbol{k})$ (left) and of $E_r^{(2)}(j, l; \boldsymbol{k})$ (right) for a photonic crystal made of a cylindrical distribution of dielectric ($\varepsilon = 8.9$) in air for TE modes.

Table 1
The 10 smallest TM and TE eigenvalues associated to the $\boldsymbol{k} = (0.4, 0)$ wavevector for the square distribution of dielectric veins in air (bottom half of Fig. 2).

	TM			TE		
	FE	FDFD	FEFD	FE	FDFD	FEFD
1	0.0782	0.0786	0.0786	0.1002	0.1005	0.1003
2	0.5615	0.5617	0.5614	0.6237	0.6238	0.6236
3	0.6286	0.6283	0.6287	0.7956	0.7951	0.7954
4	0.6456	0.6459	0.6450	0.8263	0.8264	0.8270
5	0.8897	0.8851	0.8835	0.9478	0.9479	0.9472
6	0.9681	0.9664	0.9649	1.0507	1.0513	1.0572
7	1.0363	1.0399	1.0324	1.0721	1.0773	1.0743
8	1.1159	1.1129	1.1172	1.1663	1.1680	1.1636
9	1.1314	1.1318	1.1370	1.1891	1.1841	1.1859
10	1.1856	1.1865	1.1958	1.3115	1.3105	1.3191

Nevertheless, we also investigated the behavior of the three methods calculating the 30 smallest eigenvalues. In the homogeneous case we noticed that to get a relative error of less than 10^{-3}, all three methods required roughly the same computing time (5 min for the FDFD method, 6 min for the MIT Photonic-Bands software and 7 min for the FEFD method). In the inhomogeneous case we studied the distance between the FE eigenvalues obtained by using the MIT Photonic-Bands software from our FEFD and FDFD eigenvalues, respectively. With this purpose, besides taking into account the usual photonic crystal models most considered in the literature, we considered a photonic crystal configuration consisting of three cylindrical distributions of dielectric media ($\varepsilon = 4, 3, 2$) in air (Fig. 4). In all these cases our results highlight the following:

(a) the 30 smallest eigenvalues obtained by our FDFD method are generally closer to those obtained by the FE method than those obtained by our FEFD method, for roughly the same computing time;
(b) the differences obtained by the three methods are irrelevant from the applicational point of view.

For these reasons we think that any of the three methods that we have considered could be used to validate each other. A specific field where these validations could be mandatory is the design of either photonic devices or photonic sensors in waveguides. We remark in particular that, even if the effectiveness of our FDFD and FEFD methods is essentially the same, both of them are useful for the following reasons:

(a) each method, exploiting properly the periodicity conditions, allows us to compute accurately the band spectra, at a reduced computational cost, so that they can validate each other's results;
(b) for regular grids, the choice of using either an FDFD or an FEFD method depends primarily on the user's ability to deal with finite difference or finite element methods.

The extension of the FEFD method to the 3D case, as in our FDFD method, though immediate from the theoretical point of view, is not immediately implemented. For this reason it will be considered in another paper.

Acknowledgments

Research supported by the Italian Ministry of Education and Research (MIUR) under PRIN grant No. 2006017542–003, by INdAM, and by the Autonomous Region of Sardinia under grant L.R.7/2007 "Promozione della Ricerca Scientifica e della Innovazione Tecnologica in Sardegna."

References

[1] J.D. Joannopoulos, R.D. Meade, J.N. Winn, Photonic Crystals: Molding the Flow of Light, Princeton University Press, Princeton, 2006.
[2] K. Sakoda, Optical Properties of Photonic Crystals, Springer, Berlin and New York, 2001.
[3] M. Born, E. Wolf, Principles of Optics. Electromagnetic Theory of Propagation, Interference and Diffraction of Light, sixth ed., Cambridge University Press, London, 1999.
[4] L. Brillouin, Wave Propagation in Periodic Structures, Dover Publ., New York, 1953.
[5] K. Sakoda, Optical transmittance of a two-dimensional triangular photonic lattice, Phys. Rev. B 51 (1995) 4672–4675.
[6] K. Sakoda, Transmittance and Bragg reflectivity of two-dimensional photonic lattices, Phys. Rev. B 52 (1995) 8992–9002.
[7] Pietro Contu, C. van der Mee, Sebastiano Seatzu, Fast and effective finite difference method for 2D photonic crystals, Communications in Applied and Industrial Mathematics (CAIM) (2011) http://dx.doi.org/10.1685/journal.caim.374.
[8] P. Contu, Band Structure in Photonic Crystals. Analytical and Numerical Methods, Ph.D. Thesis, University of Cagliari, 2011.
[9] Jeong-Ki Hwang, Seok-Bong Hyun, Han-Youl Ryu, Yong-Hee Lee, Resonant modes of two-dimensional photonic bandgap cavities determined by the finite-element method and by use of the anisotropic perfectly matched layer boundary condition, J. Opt. Soc. Am. B 15 (1998) 2316–2324.
[10] D.C. Dobson, An efficient method for band structure calculations in 2D photonic crystals, J. Comput. Phys. 149 (1999) 363–376.
[11] W. Axmann, P. Kuchment, An efficient finite element method for computing spectra of photonic and acoustic band-gap materials, J. Comput. Phys. 150 (1999) 468–481.
[12] G. Pelosi, A hybrid FEM-based procedure for the scattering from photonic crystals illuminated by a gaussian beam, IEEE Trans. Antennas and Propagation 48 (2000) 973–980.
[13] D.C. Dobson, J. Gopalakrishnan, J.E. Pasciak, An efficient method for band structure calculations in 3D photonic crystals, J. Comput. Phys. 161 (2000) 668–679.
[14] B.P. Hiett, J.M. Generowicz, S.J. Cox, M. Molinari, D.H. Beckett, K.S. Thomas, Application of finite element methods to photonic crystal modelling, IEEE Proc.-Sci. Meas. Technol. 149 (2002) 293–296.
[15] Woo Jun Kim, J. O'Brien, Optimization of a two-dimensional photonic-crystal waveguide branch by simulated annealing and the finite element method, J. Opt. Soc. Am. B 21 (2004) 289–295.
[16] D. Boffi, M. Conforti, L. Gastaldi, Modified edge finite elements for photonic crystals, Numer. Mat. 105 (2006) 249–266.
[17] Vu Hoang, M. Plum, C. Wieners, A computer assisted proof for photonic band gaps, Z. Angew. Math. Phys. 60 (2009) 1035–1052.
[18] M.S. Gockenbach, Understanding and Implementing the Finite Element Method, SIAM, Philadelphia, 2006.
[19] Ph.I. Davis, Circulant Matrices, Wiley-Interscience, New York, 1979.
[20] C.V.M. van der Mee, G. Rodriguez, S. Seatzu, Fast computation of two-level circulant preconditioners, Numer. Alg. 41 (3) (2006) 275–295.
[21] C. van der Mee, G. Rodriguez, S. Seatzu, Fast superoptimal preconditioning of multiindex Toeplitz matrices, Linear Algebra Appl. 418 (2006) 576–590.
[22] MIT photonic bands software, http://ab-initio.mit.edu/photons-/index.html.